Can calcium aluminates activate ternesite hydration?

M. Montes, E. Pato, P. Carmona-Quiroga, M.T. Blanco-Varela*

Instituto de ciencias de la construcción Eduardo Torroja (IETcc) (CSIC), Serrano Galvache 4, 28033 Madrid, Spain

*corresponding author: blancomt@ietcc.csic.es

Abstract

Aluminium hydroxide (AH_3) has recently been shown to be able to activate hydration in ternesite, a phase found in some calcium sulfoaluminate (CSA) cements.

This study explored the capacity of a number of calcium aluminates (C_3A, $C_{12}A_7$, CA and $C_4A_3\bar{S}$) to activate ternesite hydraulic reactivity. After laboratory synthesis, the aluminates were blended with ternesite at a ratio of 1:2 and their hydration was monitored with isothermal conduction calorimetry for 7 days at 25 ºC. The resulting pastes were analysed with XRD, FTIR and DTA. The presence of ternesite in the pastes altered the aluminate heat flow curves, shortening the induction period and bringing the reaction peak forward, an indication of hastened hydration. Ternesite also altered the reaction products, which included calcium monosulfoaluminate hydrate and strätlingite.

Keywords:

Ternesite, Calcium Aluminates, Hydration Products, Hydration Heat

1. Introduction

The mass production of portland cement (OPC) entails the consumption of vast amounts of raw materials and accounts for 4 % to 6 % of worldwide anthropogenic CO_2 emissions (0.8-0.9 t CO_2/t clinker) [1].

The cement industry is currently seeking to develop less energy-intensive, lower Greenhouse gases (GHG) emission cements. Calcium sulfoaluminate (CSA) cements, one of the most promising alternatives, are characterised by lower energy costs (at 1250 °C, the clinkering temperature is 200 °C lower than in OPC clinker) and GHG. These products emit from 25 % to 40 % less CO_2 during manufacture than OPC, depending on the composition [2]. Whilst not presently used for structural purposes due to the lack of the necessary regulation, they are commercialised as components for special mortars and concretes (such as repair or self-levelling concrete, sealing mortar or shotcrete).

The composition of the clinker in these cements may differ, although all lie in the CaO-Al_2O_3-SiO_2-Fe_2O_3-$CaSO_4$ system and have lower calcium and silicon and higher aluminate and sulfate phase contents than portland cements. The minerals present in the clinker include $C_4A_3\bar{S}$, C_2S, $C_{12}A_7$, CA, Cs and C_4AF*, although the aluminates predominate [3,4].

Ternesite, $C_5S_2\bar{S}$, which also lies within this system, is a phase compatible with ye'elemite ($C_4A_3\bar{S}$) and C_2S. It is found primarily in the crust covering the areas of portland cement kilns where the temperature is no higher than 1250 ºC and as a minority component in some CSA cements [5, 6, 10]. A calcium sulfosilicate, ternesite is formed in the reaction between anhydrite and belite. Bullerjahn et al. [6, 7] proposed a two-stage method for ternesite formation, in which clinker is synthesised at a temperature of 1250 °C and then cooled by gradually ramping the temperature down to

800 ºC. Further to recent thermodynamic predictions and empirical observation, if atmosphere (partial pressure of SO_2 and O_2) and temperature are controlled, belite- and ternesite-high sulfoaluminate clinkers can be readily produced in a single-stage process at temperatures of over 1200 ºC [8].

Although ternesite has traditionally been regarded as hydraulically inactive and of no technological interest [9], recent studies have shown that it is activated by amorphous AH_3. It hydrates, then, in their presence, yielding ettringite and C-S-H respectively the main hydration products in CSA and portland cements and the phases to which they owe their mechanical strength and durability. Strätlingite may also form with or instead of C-S-H [11].

Solubility of amorphous aluminum hydroxide in water at 25ºC is very low ([Al] ≈ $1{,}607 \times 10^{-7}$ M/l and pH 6,789; database used: concrete_3T_V07_02 and calculated with Phreeqc), it depends on the pH of medium and it rises both when pH increases or decreases from neutrality, being $Al(OH)_4^-$ the only ionic specie present at pH higher than ≈ 8,5 [11]. Solubility of ternesite is not known, but it seems that its dissolution produces hydrolysis and a pH near to 12 [12].

The solution in contact with ternesite and AH_3, contains $Al(OH)_4^-$, Ca^{2+}, SO_4^{2-}, SiO_3H^-, OH^- ions that will react when the solubility products of ettringite or strätlingite or calcium monosulfoaluminate hydrate or or C-S-H etc, are achieved; the precipitation of the said phases will consume ions in solution stimulating then new ternesite solubilisations.

Given the low water solubility of AH_3, other, more soluble aluminates might be thought to act as activators and stimulate ternesite hydration more efficiently.

Such aluminates and ternesite might be the main phases in a future CSA cement with a composition lying within the CaO-Al_2O_3-SiO_2-Fe_2O_3-$CaSO_4$ system.

The purpose of this study is to explore the capacity of a series of calcium aluminates (C_3A, $C_{12}A_7$, $C_4A_3\bar{S}$ and CA) to activate ternesite hydration, establishing the reactions involved and identifying the reaction products.

2. Experimental

Ternesite ($C_5S_2\bar{S}$), ye'elemite ($C_4A_3\bar{S}$), C_3A, $C_{12}A_7$ and CA were synthesised from stoichiometric blends of laboratory-grade $CaCO_3$, SiO_2, Al_2O_3 and gypsum ($CaSO_4 \cdot 2H_2O$). The samples were weighed, ground in a ceramic mortar, homogenised in an ethanol medium and dried at 100 °C. A pressure of 300 kp/cm^2 was applied to the powder obtained to prepare 2 cm diameter cylindrical pellets weighing approximately 4 g. The pellets were calcined at 1200 °C ($C_5S_2\bar{S}$), 1250 °C ($C_4A_3\bar{S}$), 1350 °C ($C_{12}A_7$ and CA) or 1400 °C (C_3A) for 2 h. They were subsequently ground, homogenised, dried and new pellets were prepared and calcined at the same temperatures, ternesite and ye'elemite for 6 h and the other calcium aluminates for 5 h. This process was repeated through conclusion of the synthetic reactions.

Particle size distribution in the synthesised phases was determined and recorded on a Malvern Mastersizer S particle size analyser with 632.8 nm He-Ne laser optics after subjecting samples suspended in ethanol with 5 drops of dispersant (DOLAPIX CE64 1/100) to ultrasonic dispersion for 5 min. The findings are given in Figure 1 and Table 1.

Phase purity was determined by applying Rietveld refinement to the X-ray diffraction (XRD) patterns (Table 2).

Aluminates and ternesite blend hydration (aluminate:ternesite=1:2 by mass) were monitored for 7 d at 25 ºC on a Thermometric TAM Air isothermal conduction calorimeter. Three g of sample were stirred manually with 2.1 g of water (liquid/solid ratio = 0.7) for 3 min prior to insertion in the calorimeter. Upon finalisation of the calorimetric tests, the samples were submerged in acetone to detain hydration and vacuum drying was used to remove water. The products were characterised with X-ray diffraction (XRD), IR spectroscopy (FTIR) and differential thermal analysis-thermogravimetry (DTA-TG).

The mineralogy of the synthetic phases and hydrated samples was determined on a Bruker D8 Advance X-ray diffractometer, fitted with a high voltage, 3 kW generator and a 1.54 Å CuKa anode X-ray tube operating at 40 kV and 50 mA. This instrument was coupled to a Lynxeye detector with a 3 mm anti-scatter slit and a 0.5 % Ni K-beta filter, with no monochromator.

XRD patterns of synthesized aluminates and ternesite were recorded at 5°-70º 2θ angles, with a step size of 0.01973º, and a 2 s step time. Rietveld quantitative analysis [13] was conducted on the XRD findings using GSAS software [14].

XRD patterns were recorded for the ternesite-bearing hydrated aluminates, likewise at 5°-70º 2θ angles with a step size of 0.01973º, while varying the step time to 6 s-10 s. Corundum (Al_2O_3) was added to these samples at a rate of 25 % to quantify the amorphous phase [15].

XRD scans were taken of the aluminate hydrated samples 5°-60º 2θ at a step size of 0.019746º and a 0.5 s step time.

$C_{12}A_7$+ternesite hydration was also XRD-monitored for 20 h: 5°-30° 2θ angles, step size 0.019746º and step time 0.5 s. Scans were recorded every 10 min during the first 10 h, and every 30 min from the 11^{th} through the 20^{th} hours. The paste was introduced in an air-tight sample holder to prevent carbonation and drying.

For FTIR analysis of the 7 d pastes, vacuum pressure of 10 atm was applied for 3 min to pellets prepared with approximately 1 mg of sample in 300 mg of KBr. FTIR scans were performed at frequencies of 4000 cm^{-1}-400 cm^{-1} on a Thermo Scientific Nicolet 600 FTIR spectrometer with a spectral resolution of 4 cm^{-1}. The CA and $C_{12}A_7$ pastes were also scanned after heating to 188 °C at 10 °C/min in an N_2 atmosphere.

Thermogravimetric (TG) and differential thermal (DTA) analyses were conducted on a TA Instruments Q600 TGA-DCS-DTA analyser. The samples were heated from ambient temperature to 1000 °C in a nitrogen atmosphere (100 mL/min) at a rate of 10ºC/min.

3. Results

3.1. Isothermal conduction calorimetry

The heat flow curve for ternesite alone contained only the first exothermal peak, which after 1 h had declined to 31 µW/g, given its scarce reactivity with water [6], the total heat of this reaction was very low (Figure 2 and Table 3). During hydration at 25 ºC, the heat flow curves for both the synthesised aluminates (C_3A, $C_{12}A_7$, CA, $C_4A_3\bar{S}$) and their blends with ternesite (Figure 3 and Table 3) showed an early exothermal reaction after mixing followed by a decline in the heat production rate and, in the $C_{12}A_7$, CA and

$C_4A_3\bar{S}$ samples, a second exothermal reaction that appeared earlier in the presence of ternesite.

The intensity of the initial exothermal signal in the C_3A heat flow curve tended downward for the first 7.5 h (6.6 mW/g), steadied until 10 h, continued downward until t=24 h (0.75 mW/g) and then remained flat through the rest of the test. Gismera-Diez et al. [16] reported the same pattern. In the presence of ternesite the decline was steeper and uninterrupted through 13.5 h (0.08 mW/g), after which no thermal signals were recorded.

The heat flow curves for pastes $C_{12}A_7$ and $C_{12}A_7$+ternesite contained two exothermal peaks following the very intense initial peak and an intermediate induction period. The first appeared after 1 h in both whereas the second was recorded 2.5 h earlier in the sample with than in the one without ternesite. A new, low intensity but long-lasting (9 h to 20 h) exothermal signal appeared in the sample containing ternesite. Raab et al. [17] regarded C_2AH_8 as the first product of $C_{12}A_7$ hydration, giving rise to the first visible peak on calorimetric graphs. The second peak would denote a further hydration reaction.

Induction began very quickly on the CA and CA+ternesite paste flow curves, after approximately 2 h (the second peak observed in the $C_{12}A_7$ pastes was not found here), and ended much earlier in the sample with ternesite (2.5 h and 15 h), whilst the highest reaction peak for the blended sample was recorded at 4.5 h, compared to 21 h for the sample with CA only. In addition to the aforementioned signals, the curve for paste CA showed a slight rise in heat flow between 11 h and 13 h (1 mW/g), while the slope on the CA+ternesite curve changed twice on the descending leg of the second heat flow peak, at around 11 h (1.8 mW/g) and 17 h (0.8 mW/g).

Similar behaviour was observed for the paste $C_4A_3\bar{S}$ heat flow curves. The presence of ternesite barely altered the beginning of the induction period (1.5 h) but changed the end time: the second signal peaked at 4 h, 3 h earlier than in the unblended sulfoaluminate paste. The $C_4A_3\bar{S}$ curve exhibited a slight rise in heat flow between 4 h (0.39 mW/g) and 6 h (2 W/g), in addition to the aforementioned signals. This pattern was also observed by Sánchez-Herrero et al. [18], who reported a first peak at around 4 h and a second and more intense peak at 6.5-7 h. The graph for the ternesite-bearing paste contained a low intensity exothermal signal with a peak at 1 h after the very intense initial dissolution peak, as well as a change in the slope on the descending leg of the second heat flow peak at around 9.5 h.

In the absence of ternesite, the total heat released by the 7 d, 25 ºC samples was as follows: C_3A >CA ≈ $C_{12}A_7$ > $C_4A_3\bar{S}$. In the presence of the said mineral, the order was CA > $C_{12}A_7$ > C_3A > $C_4A_3\bar{S}$ (Figure 4 and Table 4). Although the samples containing ternesite exhibited much lower heat of hydration than the unblended aluminate pastes, the total heat per gramm of aluminate increases between 19 and 91%.

3.2. XRD study

CA, $C_{12}A_7$ and C_3A hydration yields C_3AH_6, the sole stable calcium aluminate hydrate in the CaO-Al_2O_3-H_2O system, as well as a number of metastable phases (CAH_{10}, C_2AH_8, $C_4A{\cdot}xH$ (x=7, 11, 13 or 19), $C_2A{\cdot}xH$ (x= 4, 5, 7.5 or 8)) depending on the temperature and composition of the aluminate hydrated.

The diffractograms for the 7 d (25 °C) C_3A and C_3A/ $C_5S_2\bar{S}$ (1:2 by mass) blended pastes are reproduced in Figure 5. As expected, the product of C_3A hydration was katoite (C_3AH_6) [14, 16, 19]. Calcium hemicarboaluminate hydrate, ternesite, katoite,

larnite, $C_3A{\cdot}C\bar{S}{\cdot}12H$ (AFm) and portlandite traces, were identified on XRD pattern of C_3A+tenesite paste. The larnite was sourced from the original synthetic ternesite (6%C_2S). The presence of portlandite traces denoted some minor larnite hydration during the test.

The diffractogram for 7 d (25 ºC) $C_{12}A_7$ paste contained reflections attributed to C_2AH_8, CAH_{10}, gibbsite (very low intensity), and katoite, as well as the anhydrous phase. Two unidentified, low intensity lines at d=3.48 Å and d=2.61 Å were also visible on the pattern. The presence of ternesite altered $C_{12}A_7$ hydration products. Instead of the reflections observed on the pattern for $C_{12}A_7$ paste, the respective diffractogram contained lines generated by strätlingite, larnite, calcium monosulfoaluminate hydrate and ternesite (Figure 6).

The diffractogram for the 7 d (25 ºC) CA paste exhibited reflections attributed to CAH_{10} and C_2AH_8, gibbsite and katoite (low intensity), as well as to anhydrous CA. These findings were consistent with observations reported by Lothenbach et al. [21, 22]. As the most intense diffraction lines for the metastable phases C_2AH_8 and C_4AH_{19} concur at d=10.7 Å and 5.36 Å, they cannot be readily differentiated with XRD, even though the relative intensities vary somewhat. These phases are generated by dissolved ions, whereas the metastable hydrates in the $C_2A{\cdot}xH$ and $C_4A{\cdot}xH$ series are obtained by dehydration of the ions carrying the most water.

The shift observed here in the main reflections for C_2AH_8 (d=10.7 Å and 5.36 Å) to slightly lower values (d=10.4 Å and 5.2 Å) on the diffractograms for pastes $C_{12}A_7$ and CA may denote slight sample dehydration due to their exposure to acetone and vacuum drying to detain hydration and remove water [23].

As in $C_{12}A_7$, the presence of ternesite altered CA hydration products. The diffractogram for the blended paste contained none of the reflections observed on the pattern for CA paste, although lines indicative of strätlingite, calcium monosulfoaluminate hydrate, larnite and ternesite were identified (Figure 7).

The $C_4A_3\bar{S}$ hydration products identified by XRD were AFm and gibbsite (Figure 8), a finding consistent with prior reports [24]. The hemicarboaluminate identified was deemed to be due to sample weathering. Part of the $C_4A_3\bar{S}$ was still anhydrous after 7 days of hydration at 25 ºC. The presence of ternesite appeared to stimulate $C_4A_3\bar{S}$ dissolution, inasmuch as no reflections for this phase were observed on the diffractogram. Here AFm was the reaction product, while no reflections from crystalline aluminium hydroxide was observed.

The mineralogical analysis of the hydrated ternesite-containing aluminates based on quantitative XRD is given in Table 5.

3.3. In-situ XRD

The reactions taking place over time in paste $C_{12}A_7$+ternesite generated a heat flow curve with a number of signals. These reactions were identified by continuous XRD scanning during the first 20 h of hydration (Figure 9). The intensity of the reflections attributed to C_2AH_8 rose over time, whilst the intensity of the lines for $C_{12}A_7$ and ternesite declined.

The decline in intensity of the main diffraction lines for $C_{12}A_7$ and ternesite concurred in time with the first exothermal peak on the calorimetric curve, an indication that these phases dissolved very early into hydration. C_2AH_8 was identified as the first hydrate, generated at 10 min, along with φ-AH_3 (Equation 1). After 1 h (small exothermal peak

on the calorimetric curve), the intensity of the diffraction lines for $C_{12}A_7$ and ternesite declined again, while that of the C_2AH_8 reflections continued to rise. The two reagents declined throughout the induction period. A new phase, $CaAl_2Si_7O_{18}\cdot 3.5H_2O$, appeared after 4.5 h through the end of the test (20 h) as a product of the reaction between ternesite and φ-AH_3. Phase φ-AH_3, which was identified from the outset, began to gradually decline after 2 h and disappeared entirely after 5 h, as strätlingite and $CaAl_2Si_7O_{18}\cdot 3.5H_2O$ formed.

$$C_{12}A_7 + 51\ H_2O \rightarrow 6C_2AH_8 + AH_3 \quad (1)$$

The strätlingite reflections (Equation 2) were identified after 5 h, as C_2AH_8 continued to rise and ternesite and $C_{12}A_7$ to decline as a result. The absence of reflections for new crystalline sulfates may be explained either by their low crystallinity (with the probable formation of AFm nuclei) or the fact that the sulfate ion resulting from ternesite decomposition remains in solution after strätlingite crystallisation.

$$2AH_3 + 2C_2S\cdot C\bar{S} + 10H \rightarrow 2C_2SA\cdot 8H_2O + 2C\bar{S} \quad (2)$$

Calcium monosulfoaluminate hydrate (Equation 3) appeared at around 9 h-10 h, however, concurring with the low intensity, long-lasting exothermal shoulder on the calorimetric curve.

$$3C_2A\cdot 8H_2O + 2C\bar{S} + 3H_2O \rightarrow 2C_3A\cdot C\bar{S}\cdot 12H + AH_3 \quad (3)$$

The same sample was scanned after storage for 7 d in a moist environment at 25 ºC. The diffractogram showed higher intensity strätlingite reflections and AFm phases, whilst no lines for the intermediate phase, $CaAl_2Si_7O_{18}·3.5H_2O$, were observed. The intensity of the ternesite and C_2AH_8 reflections was low, although the latter was still visible. These findings differed in some respects from the 7 d (25 ºC) calorimetric results, where large amounts of unreacted ternesite were observed and no C_2AH_8 was identified.

The explanation for the differences between the XRD findings for the sample hydrated for 7 d in the calorimeter and the one hydrated for 20 h in the diffractometer and subsequently stored at 25 ºC for 6 d more, might be that in the latter, the incidence of the X-rays on the sample may have induced a temperature substantially higher than 25 ºC. That may have given rise to different phases than obtained at a constant 25 ºC and would also explain why the ternesite was largely consumed in 20 h in the diffractometer whereas a large fraction of the mineral had not reacted after 7 d at 25 ºC in the calorimeter.

3.4. FTIR study

The FTIR analyses (Table 6) confirmed the XRD results. The infrared spectrum for paste C_3A exhibited the absorption lines characteristic of katoite, some (in the 790 cm^{-1}-820 cm^{-1} and 520 cm^{-1}-530 cm^{-1} ranges) overlapping with the signals for the remaining anhydrous C_3A [16]. Slight carboaluminate contamination was likewise observed.

The most intense bands on the FTIR for paste $C_4A_3\bar{S}$, in the O-H stretching zone (4000 cm^{-1}-3000 cm^{-1}) were generated by overlapping AFm and gibbsite signals [18]. On the rest of the spectrum the bands for these two hydrates were observed to overlap

295 with those of anhydrous $C_4A_3\bar{S}$ and, to a lesser extent, calcium hemicarboaluminate
296 hydrate (Hc).

297 The spectra for pastes CA and $C_{12}A_7$ exhibited similar bands in the 4000 cm^{-1}-
298 2500 cm^{-1} range, although they were sharper in the former, where they were attributed
299 to gibbsite overlapping with katoite, CAH_{10} and C_2AH_8. Overlapped bands generated by
300 CAH_{10}, C_2AH_8 (more intense in $C_{12}A_7$) and gibbsite (much more intense in CA)
301 appeared in the 1300 cm^{1}-400 cm^{-1} zone. Some of the bands on these spectra were
302 identified by Fernández-Carrasco et al. [25]. In order to identify more clearly the phases
303 present, these samples were thermally treated at 188ºC, temperature at which CAH_{10}
304 phase is decomposed and C_2AH_8 partially lose the water.

305 After the two pastes were heated to 188 °C, the FTIR spectra changed radically: the
306 CAH_{10} bands disappeared and the C_2AH_8 bands were altered due to a partial water loss.
307 The gibbsite bands intensified on the paste CA spectrum and nearly disappeared in
308 $C_{12}A_7$, where the signals for katoite and partially dehydrated C_2AH_8 intensified. These
309 findings infer that the two pastes contained the same hydrates, albeit in different
310 proportions. CA had more gibbsite and less katoite and C_2AH_8 than $C_{12}A_7$.
311 The bands attributable to ternesite stood out on the spectra for the four aluminate pastes
312 containing the mineral. They appeared in all the samples at 1153 cm^{-1}, 1121 cm^{-1},
313 947 cm^{-1}, 878 cm^{-1}, 837 cm^{-1}, 660 cm^{-1}, 630 cm^{-1}, 602 cm^{-1}, 541 cm^{-1} and 517 cm^{-1} [26],
314 i.e., in the 1300 cm^{-1}-400 cm^{-1} range, where no other anhydrous phase absorptions were
315 observed. All four spectra exhibited a narrow, intense absorption signal at 424 cm^{-1} and
316 other wider, overlapping signals at around 520 cm^{-1} and 540 cm^{-1}, characteristic of a
317 number of calcium aluminate hydrates. The ternesite spectrum (multiplied by a factor of
318 0.4-0.8) was subtracted from the original paste spectra to better identify the hydrates.

The spectra for paste C_3A+ternesite (Figure 10) exhibited bands in the O-H stretching vibrations zone mainly generated by the presence of Hc overlapped with bands from AFm and portlandite while the O-H stretching band from katoite was not clearly ditinguisted, After subtracting ternesite spectra, the most prominent bands in the 1300-400 cm^{-1} range were attributed to AFm (at ≈1110, 784, 539, 424 cm^{-1}) and Hc.

The spectrum for paste $C_{12}A_7$+ternesite (Figure 11) exhibited O-H stretching vibrations generated by water and hydrates, attributed to AFm (3670 cm^{-1}), as well as a wide band with two peaks, at 3615 cm^{-1} and 3530 cm^{-1} (possibly indicative of a weathering-induced hemicarboaluminate). The bands remaining after the ternesite spectrum was subtracted, all in the 1300 cm^{-1}-400 cm^{-1} range, were attributable to C_2ASH_8 (1013 cm^{-1}, 964 cm^{-1}, 710 cm^{-1}) or AFm (780 cm^{-1}, 572 cm^{-1}, 539 cm^{-1}). A band overlapping generously with ternesite attributable to AFm was observed in the sulfate ν_3 zone.

The spectra for paste CA+ternesite (Figure 12) were very similar to the ones for $C_{12}A_7$+ternesite, with O-H stretching vibrations from water and hydrates attributed to AFm (3670 cm^{-1}), although an intense band appeared at 3622 cm^{-1}, along with a wide band at 3559 cm^{-1}-3487 cm^{-1}, which overlapped with another at 3550 cm-1, which could be assigned to AH_3. The bands observed in the 1300 cm^{-1}-400 cm^{-1} range on the post-subtraction spectrum at around 1013 cm^{-1}, 964 cm^{-1} and 710 cm^{-1}, attributable to C_2ASH_8, were much more intense than on the $C_{12}A_7$ spectrum. Less intense bands generated by AFm were found at 780 cm^{-1}, 572 cm^{-1} and 539 cm^{-1}.

The spectra for paste $C_4A_3\bar{S}$+ternesite (Figure 13) also contained O-H stretching

vibrations from water and hydrates that concurred with the signals for gibbsite, although

their relative intensities differed. The most prominent band in the 1300 cm^{-1}-400 cm^{-1} range on the spectrum resulting from subtracting the ternesite bands, at 1020 cm^{-1}, was characteristic of gibbsite, which had not been identified by XRD. Signals attributed to AFm were observed at 780 cm^{-1}, 582 cm^{-1} and 539 cm^{-1}.

3.5. DTA-TG study

The water content in 7 d aluminate pastes was: CA> $C_{12}A_7$>$C_4A_3\bar{S}$ >C_3A. The order for the pastes containing ternesite (normalised per g of dry aluminate), which held less water, was CA>$C_{12}A_7$ >C_3A >$C_4A_3\bar{S}$ (Figure 14).

Assigning thermal signals to calcium aluminate hydrate dehydration/dehydroxylation in poly-phase samples is a complex task, for each phase holds various forms of bound water, which may be gradually released with rising heat. As a result, each phase generates several endothermal signals in the same temperature ranges, which explains the lack of uniformity in the literature cited in Table 7.

The most prominent, i.e., most intense and sharpest, of the endothermal dehydration and dehydroxylation peaks for the hydrates in the pastes studied was attributed to katoite, at 300 °C on the DTA curve for paste C_3A. This peak was also observed, vaguely and overlapping with gibbsite, on the curves for pastes CA and $C_{12}A_7$.

Further to the TG findings, hydrated paste C_3A contained 79 wt% katoite and 21 wt% anhydrous C_3A. In other words, the hydration rate in C_3A was 0.73.

The DTA curves for pastes CA and $C_{12}A_7$ (Figure 15) exhibited several thermal signals at temperatures of under 200 °C and in the 200 °C-600 °C range, all associated with weight loss on the TG/DTG curves (Figure 14). In the first range of temperatures the

368 intense endothermal peaks at around 80 °C-88 °C were attributed to amorphous AH_3
369 [33]. They overlapped with a peak at around 100 °C-110 °C, generated by water loss
370 from CAH_{10} and the water physically adsorbed on the C_2AH_8 interlayer. Another
371 endothermal signal at around 145 °C-160 °C could be attributed to further partial water
372 loss from C_2AH_8 [35]. In the second temperature range, the DTA curves for both pastes
373 exhibited endothermal signals of varying intensity at around 260 ºC, 280 ºC and 320 ºC,
374 attributed to water loss from C_2AH_8, AH_3 and C_3AH_6. Two much less intense signals at
375 421 ºC and 524 ºC were also attributed to those phases.
376
377 The DTA curves for sample $C_4A_3\bar{S}$ (Figure 16) contained very intense <200 °C signals:
378 at 120 and 180 °C for AFm and 120 °C overlapped with hemicarboaluminate, the latter
379 due to sample weathering. Three peaks were observed at 200 °C-300 °C, the most
380 intense at 264 °C and the others at 224 °C and 286, which might be due to AFm, Hc and
381 gibbsite overlapping. The peak at 286 °C was associated with gibbsite water loss.
382
383 C_3A+ternesite curve (Figure 17) contained an intense broad (120-180ºC) endothermal
384 signal, peaking at around 154 ºC and other broad one at 240 ºC, denoting water loss
385 from Hc and AFm. The signal at 285 °C was generated by Katoite and the final one at
386 412°C by portlandite, as per Torréns-Martín et al. [39].
387 Curves for CA, $C_{12}A_7$ and C_4A_3S with ternesite pastes exhibited a very intense
388 endothermal signal at around 170 °C-180 °C generated by water loss from AFm phases.
389
390 The curves for samples CA+ternesite and $C_{12}A_7$+ternesite (Figure 18) had endothermal
391 signals of varying intensity at around 125 °C-128 °C, 170 °C and 220 °C, attributable to
392 strätlingite, according to Kuzel [36] and Matschei [40], and as regards the signal at
393 170 °C, also to AFm. The conclusion that could be drawn from a comparison of the

intensity of these signals is that CA+ternesite had a higher proportion of strätlingite and paste $C_{12}A_7$+ternesite a higher proportion of AFm. That finding is consistent with the FTIR and XRD results. These two pastes also exhibited a much lower intensity endothermal signal at 285 °C that might be associated with AH_3 water loss, although the XRD analyses failed to identify that phase.

In addition to the aforementioned AFm and hemicarboaluminate signals at 170 °C, 210 °C and 110 °C, the $C_4A_3\bar{S}$+ternesite sample exhibited others attributable to gibbsite overlapped with AFm, which generated two peaks, at 250 °C and 290 °C (Figure 19).

4. Discussion

The calorimetric curves for the hydrated aluminate pastes contained a first dissolution peak, followed by an induction period and an intense reaction peak in pastes CA, $C_{12}A_7$ and $C_4A_3\bar{S}$ [17, 18, 21] The presence of ternesite in the pastes altered the calorimetric curves in all cases, shortening the induction period and bringing the reaction peak forward.

The pastes containing $C_{12}A_7$ had a much more active induction period than any of the others, with a heat flow a full order or magnitude higher. C_2AH_8 and φ-AH_3 formed from the onset of hydration in pastes with ternesite, which reacted with φ-AH_3 in the induction period, giving rise to an intermediate phase, $CaAl_2Si_7O_{18}\cdot 3.5H_2O$. In the main exothermal peak concurred the consumption of all the φ-AH_3 and the first strätlingite crystallization, while C_2AH_8 precipitation as well as reagents dissolution (ternesite and $C_{12}A_7$) continued. The main reaction peak was followed by calcium monosulfoaluminate hydrate precipitation. $C_{12}A_7$ can therefore be regarded to powerfully activate ternesite, which dissolved from the outset, giving rise to calcium

420 silicoaluminate hydrate precipitation even prior to calcium monosulfoaluminate
421 precipitation.
422 Whilst the 7 d aluminate+ternesite (1:2) pastes released less total heat than the
423 analogous unblended aluminate pastes, however when total heat was expressed per unit
424 of mass of aluminate, the four samples containing ternesite exhibited higher values than
425 their unblended aluminate counterparts. The inference is that ternesite participate in the
426 hydration reactions and not only hastened but activated aluminate hydration. In the
427 presence of ternesite, the amount of heat per aluminate mass unit rose by 91 % in CA,
428 87 % in $C_{12}A_7$, 19 % in C_3A and 36 % in $C_4A_3\bar{S}$ (Table 4).
429 Ternesite is activated when hydrated in the presence of C_3A, $C_{12}A_7$ and CA, accounting
430 for 43 wt% to 22 wt% of the respective pastes, according to XRD data. On the grounds
431 of the quantitative XRD findings in conjunction with the total mass loss at 1000 °C
432 determined with TG, 16 wt% of the ternesite reacted in C_3A, 50 wt% in CA and 53 wt%
433 in $C_{12}A_7$. Those results denote scant (2 %) ternesite reaction in the ternesite-ye'elemite
434 blended paste.
435 C_3A hydration, which was incomplete after 7 d (hydration degree = 0, 73), yielded
436 katoite (Equation 4). Further to the XRD findings, C_3A hydration in the presence of
437 ternesite produces a small amounts of katoite (5.36 wt%) calcium monosulfoaluminate
438 hydrate (1.76 wt%) and calcium hemicarboaluminate hydrate (6.91 wt%) as well as
439 larnite (1.71 wt%), ternesite (43.11 wt%), C_3A (0.72 wt%) as the main crystalline
440 phases and amorphous phases (40.42 wt%).
441

$$C_3A + 6H_2O \rightarrow C_3AH_6 \quad (4)$$

442

443 Calculus derivated from DRX an TG data reveal a scant reaction of ternesite (16,3 wt%)
444 while C_3A reacted almost completely (97 wt%). These data fit very well with the
445 increment of the total heat released per aluminate mass unit in this paste (Table 4).
446
447 Taken into account the loss of mass recorded by TG, it can be concluded that C_3A plus
448 ternesite paste contains 28,7 wt % of AFm+Hc; 11,5 wt% of C_3AH_6 and 1,6 wt% de
449 portlandita; these values are very much more higher than those determined by XRD,
450 which would be an indication of the poor crystallinity of the hydrates obtained.
451 Pastes $C_{12}A_7$ and CA gave rise to the same hydration products, CAH_{10}, C_2AH_8 and AH_3,
452 although in different proportions, in addition to the respective anhydrous aluminates. In
453 the presence of ternesite the anhydrous aluminates reacted fully, generating AFm and
454 C_2ASH_8 in both cases. No other calcium aluminate hydrate appeared as a crystalline
455 phase.
456 Combining TG and XRD data the amount of ternesite consumed in samples $C_{12}A_7$ +
457 ternesite and CA + ternesite, is respectively 53% and 50%; assuming that all the sulfate
458 of the dissolved ternesite forms AFm and all the remaining aluminum forms strätlingite,
459 the proportions of these phases was calculated which are shown in Table 8. Both
460 hydrates would be in much higher proportion than that shown by XRD, however the
461 results are consistent with the mass loss observed by TG, which would account for the
462 poor crystallinity of AFm and strätlingite in said pastes.
463 The hydration products for paste $C_4A_3\bar{S}$ included AFm (33 %) and AH_3 (43 %) (small
464 signal of hemicarboaluminate was also observed) (Eq.5).
465

$$C_4A_3\bar{S} + 12H_2O \rightarrow C_4A\bar{S}H_{12} + 2AH_3 (+ C_4AcH_{11}) \quad (5)$$

466
467 The XRD and TG findings showed that in the presence of ternesite, around 3 wt % of
468 the ye'elemite remained unreacted. AFm appeared and AH_3 was identified by FTIR and

469 DTA, although not on the X-ray diffractograms, an indication of its amorphous nature.
470 These findings do not infer that ye'elemite acted as a ternesite activator, for no
471 strätlingite was identified. As noted earlier, further to calculations based on the ternesite
472 content (50.5 wt%), the total TG-determined mass loss (17.6 wt%) and the
473 ye'elemite:ternesite ratio, the sample contained 97.8 % of the ternesite initially added.
474 That was very likely due to the common sulfate ion effect, which delayed ternesite
475 dissolution. Under such circumstances, ternesite would affect the crystallinity of the
476 AH_3 formed (gibbsite in the ye'elemite paste and amorphous aluminium hydroxide in
477 yeelemite+ ternesite paste) and the ye'elemite hydration rate (shortening the induction
478 period), but the amount of ternesite consumed along the reaction time was very low.
479 The calorimetric data nonetheless revealed a 36 % rise in the total heat per unit of
480 aluminate released, perhaps due to the filler effect.
481 The crystalline AFm of ternesite plus ye'elemite paste content was also very low,
482 inasmuch as 96 wt % of the ye'elemite reacted. The hydrate content determined with
483 XRD and the calculated using the degree of reaction for ternesite and ye'elemite is
484 given in Table 8. The table also lists the mass loss in the four pastes at 1000 ºC
485 calculated from those data and from the TG findings.
486 As XRD identified crystalline AH_3 in the ternesite-free paste but not in the paste
487 bearing ye'elemite + TER, the presence of ternesite may be deduced to have affected
488 both AFm and AH_3 crystallinity.
489
490 The XRD-determined crystalline AFm content in the pastes was much lower than would
491 be expected on the grounds of the reaction degree of ternesite and aluminates. The
492 calculated loss of evaporable matter in the hydrates was much higher than calculated
493 with the XRD data and very close to the TG findings. A substantial portion of the AFm

may consequently be assumed to be scantly crystalline and included in the amorphous phase determined in XRD patterns.

5. Conclusions

This study explored the possible activation of ternesite hydration by a series of aluminates by recording heat of hydration and analysing the 7 d hydration products with XRD, FTIR and DTA. The ultimate aim was to pave the way for the future development of a new eco-clinker, in which one of the main minerals would be ternesite blended with aluminates that would activate its hydration. The major conclusions are listed below.

- Ternesite was activated in all the blends, although with varying intensity depending on the aluminate added. Aluminate efficacy was, in descending order, $C_{12}A_7 \approx CA > C_3A >>>> C_4A_3\overline{S}$.

- The presence of ternesite in the pastes altered the aluminate heat flow curves, shortening the induction period and bringing the reaction peak forward, an indication of hastened hydration. The calorimetric findings revealed rises of 19 % to 91% in total heat release per unit of aluminate mass, attesting to the activation of aluminate hydration in the presence of ternesite.

- Hydration of C_3A produces Katoite as the only hydration product but in presence of ternesite the katoite amount is hardly reduced while AFm and Hemicarboaluminate were found.

519 - $C_{12}A_7$ and CA were analysed jointly, for they yielded the same hydration products.
520 These aluminates activated ternesite hydration and their pastes contained the same
521 phases (AFm and stratlingite), albeit in different proportions..
522
523 - Due to the common sulfate ion effect, much less ternesite (2 wt%) was consumed in
524 paste $C_4A_3\bar{S}$ than in any of the other samples. However ternesite alter the cristallinity of
525 the obtained hydrates; scantly crystalline AFm and amorphous AH_3 were the main
526 hydration products in this paste. As no strätlingite was obtained, ternesite could not be
527 regarded as having been clearly activated by ye'elemite, despite some calorimetric
528 evidence to that effect.
529 **Acknowledgements**.
530
531 This paper has been funded from BIA2016-76466-R project as well as the Regional
532 Government of Madrid Community and European Social Fund (Geomaterials
533 Programme2 S2013/MIT-2914). Authors thank to Ministerio de Economía y
534 Competitividad the young resercher contract given to Myriam Montes. Financial
535 support for Dr. Paula M. Carmona-Quiroga's participation was provided by the Spanish
536 Ministry of the Economy and Competitiveness under project BIA2015-73237-JIN.
537
538 **References**
539 [1] O. Edenhofer, et al. IPCC, 2014: Climate Change 2014: Mitigation of Climate
540 Change. Contribution of Working Group III to the Fifth Assessment Report of the
541 Intergovernmental Panel on Climate Change (2014)
542 [2] Marta García Maté. Processing and Characterisation of calcium sulphoaluminate
543 (CSA) eco-cement with taylored performances. (2014) PhD University of Málaga

544 [3] M. Carmen Martín-Sedeño, Antonio J.M. Cuberos, Ángeles G. De la Torrea, Gema
545 Álvarez-Pinazo, Luis M. Ordónez; Milen Gateshkic, Miguel A.G. Aranda. Aluminum-
546 rich belite sulfoaluminate cements: Clinkering and early age hydration. Cement and
547 Concrete Research Volume 40, Issue 3, March (2010) 359–369
548 [4] K. Morsli, A.G. de la Torre, M. Zahir, M.A.G. Aranda. Mineralogical phase analysis
549 of alkali and sulfate bearing belite rich laboratory clinkers. Cem. Concr. Res., 37 (2007)
550 639–646
551 [5] M.Marroccoli, F.Montagnaro,M.L. Pace, A. Telesca, G.L. Valenti, Synthesis of
552 calcium sulfoaluminate cements from blends of coal combustion ashes with flue gas
553 desulfurization gypsum, PTSE, Ischia, Italy, 2010.
554 [6] Bullerjahn, F., Zajac, M. & Ben Haha, M. CSA raw mix design: effect on clinker
555 formation and reactivity. Materials and Structures, Volume 48, (2015) 3895-3911.
556 [7] Bullerjahn, F., Schmitt, D. & Ben Haha, M. Effect of raw mix design and of
557 clinkering process on the formation and mineralogical composition of (ternesite) belite
558 calcium sulphoaluminate ferrite clinker.Cement and Concrete Research, Volume 59,
559 (2014) 87-95.
560 [8] T. Hanein, I. Galan, F. P. Glasser, S.Skalamprinos, A. Elhoweris, M.S. Imbabi, M.N.
561 Bannerman, Stability of ternesite and the production at scale of ternesite-based clinkers
562 Cement and Concrete Research 98 (2017) 91–100
563 [9] Sherman, N., Beretka, J., Santoro, L. & Valenti, G. L. Long-term behaviour of
564 hydraulic binders based on calcium sulfoaluminate and calcium sulfosilicate. Cement
565 and Concrete Research (CCR), Volume 25, (1995)113-126.
566 [10] .B. Pliego-Cuervo, F.P. Glasser, The role of sulphates in cement clinkering:
567 subsolidus phase relations in the system CaO–Al2O3–SiO2–SO3. Cem. Concr. Res., 9
568 (1979) 51–56

[11] Mohsen Ben Haha, Frank Bullerjahn, Maciej Zajac "On the reactivity of ternesite" XIV ICCC, Pekín 2015

[12] Peter K. Holt, Geoffrey W. Barton, Mary Wark, Cynthia A. Mitchell. A quantitative comparison between chemical dosing and Electrocoagulation.Colloids and Surfaces A: Physicochem. Eng. Aspects 211 (2002) 233-248.

[13] H.M. Rietveld, A profile refinement method for nuclear and magnetic structures, J. Appl. Crystallogr. 2 (1969) 65–71.

[14] A.C. Larson, R.B. Von Dreele, General Structure Analysis System (GSAS) program, Rep. No. LA-UR-86748, Los Alamos National Laboratory, Los Alamos, CA, 1994.

[15] M. A. G. Aranda, A. G. De la Torre. Rietveld Quantitative Phase Analysis of OPC Clinkers, Cements and Hydration Products. Reviews in Mineralogy & Geochemistry Vol. 74 pp. 169-209 (2012)

[16] S. Gismera-Diez, B. Manchobas-Pantoja, P.M. Carmona-Quiroga, M.T. Blanco-Varela, Effect of BaCO3 on C3A hydration Cement and Concrete Research, 73 (2015) 70-78.

[17] B. Raab, H. Poellmann, Heat flow calorimetry and SEM investigations to characterize the hydration at different temperatures of different 12CaO·Al2O3 (C12A7) samples synthesized by solid state reaction, polymer precursor process and glycine nitrate process Thermochimica Acta 513 (2011) 106–111

[18] M.J. Sánchez-Herrero, A. Fernández-Jiménez, A. Palomo, $C_4A_3\bar{S}$ hydration in different alkaline media, Cement and Concrete Research 46 (2013) 41-49

[19] E. Breval, C3A Hydration, Cement and Concrete Research, 6 (1976)129-138

[20] J.I. Bhatty, A review of the application of thermal analysis to cement-admixture, Systems Thermochimica Acta 189 (1991) 313-350

[21] S.R. Klaus, J. Neubauer, F. Goetz-Neunhoeffer, Hydration kinetics of CA2 and CA—Investigations performed on synthetic calcium aluminate cement, Cement and Concrete Research 43 (2013) 62–69

[22] B. Lothenbach, L. Pelletier-Chaignat, F. Winnefeld, Stability in the system CaO–Al2O3–H2O, Cement and Concrete Research 42 (2012) 1621-1634

[23] T.R. Jensena, A. Nbrlund Christensenb, J.C. Hansonc, Hydrothermal transformation of the calcium aluminum oxide hydrates CaAl2O4d·10H2O and Ca2Al2O5d·8H2O to Ca3Al2(OH)12 investigated by in situ synchrotron X-ray powder diffraction, Cement and Concrete Research 35 (2005) 2300-2309

[24] F.P. Glasser, L. Zhang, High-performance cement matrices based on calcium sulfoaluminate–belite compositions, Cement and Concrete Research 31 (2001) 1881–1886

[25] L. Fernández-Carrasco, D. Torrens-Martín, L.M. Morales, S. Martínez- Ramírez, Infrared Spectroscopy in the Analysis of Building and Construction Materials, Infrared Spectroscopy, Materials Science, Engineering and Technology (2012) 369-382

[26] N.V. Chukanov, Infrared spectra of mineral species (2014) Ed Springer

[27] S.M. Bushnell-Watson, J.H. Sharp, The application of thermal analysis to the hydration and conversión Reactions of calcium aluminate Cements, Materiales de construcción 42 (1998) 13-32

[28] C.M.George, Industrial alumina cement, Structure and Performance of Cement (1983) 415

[29] L. Fernandez Carrasco, Procesos de hidratación y carbonatación del cemento de aluminatos de calcio; influencia de los álcalis. Alteraciones microestructurales y relación con sus propiedades mecánicas. Thesis Instituto de la Construcción Eduardo Torroja, Madrid, Spain, 2000

[30] N. Ukrainczyk, T. Matusinovic, S. Kurajica, B. Zimmermann, J. Sipusic, Dehydration of a layered double hydroxide—C2AH8N, Thermodinamic Acta 464 (2007) 7-15

[31] V.S. Ramachandran, Thermal analysis of cement components hydrated in the presence of calcium carbonate, Thermodinamic Acta 127 (1988) 385-394

[32] P.A. Barnes, D.J. Baxter, A critical analysis of the application of derivative thermogravimetry to the determination of the degree of conversion of high alumina cement, Thermochimica Acta 24 (1978) 427-431

[33] J. Szczerba, D. Madej, E. Sniezek, R. Prorok, The application of DTA and TG methods to investigate the non-crystalline hydration products of CaAl2O4 and Ca7ZrAl6O18 compounds, Thermochimica Acta 567 (2013) 40– 45

[34] C. Gosselin, Microstructural Development of Calcium Aluminate Cement Based Systems with and without Supplementary Cementious Materials, Thesis École Polytechnique Fédérale de Lausanne, Lausanne, Switzerland (2009)

[35] V.S. Ramachandran, R.M. Paroli, J.J. Beaudoin, A.H. Delgado, Handbook of Thermal Analysis of Construction Materials, ed.W.A.Publishing.2003, Norwich, New York, U.S.A

[36] H.J. Kuzel, Crystallographic data and thermal decomposition of synthetic gehlenite hydrate 2CaO·Al2O3·SiO2·8H2O, Neues Jahrbuch fuer Mineralogie Monatshefte 148 (1976) 319-325

[37] T. Danner, H. Justnes, M. Geiker, R.A. Lauten, Early hydration of C3A–gypsum pastes with Ca- and Na-lignosulfonate, Cement and Concrete Research 79 (2016) 333-343

642 [38] F. Sáez del Bosque I. Modificaciones nanoestructurales en pastas de cemento.
643 Thesis Instituto de Ciencias de la Construcción Eduardo Torroja (CSIC) and
644 Universidad Autonoma de Madrid, Madrid, Spain (2012).
645 [39] D. Torréns-Martín, L. Fernandez-Carrasco, M.T. Blanco-Varela, Thermal analysis
646 of blended cements, Journal of Thermal Analysis calorimetric 121 (3) (2015)
647 [40] T. Matschei. Thermodynamic properties of Portland cement hydrates in the system
648 CaO–Al2O3–SiO2–CaSO4–CaCO3–H2O, Cement and Concrete Research 37 (2007)
649 1379-1410
650

651

652 Table 1. Particle size distribution parameters determined by laser diffraction
653

µm/%	C_3A	CA	$C_{12}A_7$	$C_4A_3\bar{S}$	$C_5S_2\bar{S}$
d_{90}	100	100	76.5	78	89.5
d_{50}	93.5	99.3	66.4	46	85
d_{10}	31	57	34	14	43.5
$D_{4.3}$	21.17	11.52	59	59.14	35.13
Span	2.41	3.17	8.25	1.99	8.29
RRSB	0.74	0.97	2.36	0.62	2.48

654
655 Table 2. Quantitative mineralogical analysis of the phases synthesised
656

wt%	$C_5S_2\bar{S}$	C_2S	C_3A	$C_{12}A_7$	CaO	CA	$C_4A_3\bar{S}$	$C\bar{S}$	Rwp
$C_5S_2\bar{S}$	94	6							10
C_3A			100						16.52
$C_{12}A_7$				99.82	0.18				16.99
CA				2.52		97.48			14.12
$C_4A_3\bar{S}$				1.30			97.98	0.70	15.63
ICSD card	85123	81096	1841	241243	52783	260	80361	16382	

657
658 Table 3. Data for the heat flow curves shown in Figure 3
659

	Initial peak 1	Peak 2 maximum		Min induction period		Peak 3 maximum		Maximum exothermal signal	
	Heat flow (mW/g)	t (h)	Heat fl. (mW/g)	t (h)	Heat fl. (mW/g)	t(h)	Heat fl. (mW/g)	t(h)	Heat fl. (mW/g)
C_3A	180	-	-	-	-	-	-	-	-
C_3A+ter	120	-	-	-	-	-	-	-	-
$C_{12}A_7$	159	1	20	5.5	9.0	8.5	13	-	-
$C_{12}A_7$+ter	134	1	8.9	3	6.3	5	10	13.5	1.8
CA	99	-	-	2.5	0.39	21	27	12	1
CA+ter	121	-	-	2	0.39	4.5	24	17	0.8
$C_4A_3\bar{S}$	71	-	-	2.8	0.33	7	114	-	-
$C_4A_3\bar{S}$+ter	23	1	1.3	2	1	4	28	9.5	1.1
Ternesite	117	-	-	-	-	-	-	-	-

660
661
662

663 Table 4. Experimental total heat (J/g aluminate) in 7 day pastes hydration (25ºC)
664

	Experimental total heat	ΔQ
Ternesite	43 J/g	
CA	563 J/g	
CA+Ternesite	1076 J/g	91%
$C_{12}A_7$	557 J/g	
$C_{12}A_7$+Ternesite	1043 J/g	87%
$C_4A_3\bar{S}$	464 J/g	
$C_4A_3\bar{S}$+Ternesite	630 J/g	36%
C_3A	744 J/g	
C_3A+Ternesite	885 J/g	19%

665
666
667 Table 5. Quantitative mineralogical analysis of blended aluminate + ternesite pastes
668

wt%	$C_5S_2\bar{S}$	C_2S	C_3A	$C_4A_3\bar{S}$	C_2ASH_8	AFm	C_3AH_6	Hc	% amorphous	Rwp
C_3A+ $C_5S_2\bar{S}$	43,11	1.71	0.72			1.76	5.36	6.91	40.42	11.31
$C_{12}A_{7+}$ $C_5S_2\bar{S}$	22.62	2.70			24.84	11.61			38.23	11.20
$C_4A_3\bar{S}$+$C_5S_2\bar{S}$	50.51	1.66		0.99		10.63		1.11	35.1	8.80
CA+ $C_5S_2\bar{S}$	23.29	2.21			35.95	5.84			32.71	11.62
ICSD card	85123	81096	1841	80361	69413	100138	202316	263124		

669
670

Table 6. Absorption bands on FTIR spectra for 7 d (25 °C) pastes. s=Strong, vs=very strong, w=weak, vw=very weak

Paste C_3A	Paste $C_4A_3\bar{S}$	Paste CA	Paste $C_{12}A_7$	Attributed to
		3682	3682	
	3676 vw			AFm/Hc
3660 s				C_3AH_6
	3620 w	3620	3620	AH_3
3543 vw				C_3AH_6
	3526 w	3526	3526	AH_3
3523 vw				
	3467 w	3467	3467	AH_3/C_2AH_8
	1167 w			AFm
	1115-1108 s			AFm
	1024 s	1024	1024	AH_3
	968 w	968		AH_3
899 w				C_3A
865 w		865	865	$C_3A/CAH_{10}/C_2AH_8$
809 s				C_3AH_6/C_3A
	786 s			AFm
		777	777	
		710	710	C_2AH_8
		636		
	617 w			
		578	578	CAH_{10}
521 s	528 vs	528	528	CAH_{10}/ C_3A C_2AH_8/AFm
	422 s	422	422	CAH_{10}/ C_2AH_8/AFm

Table 7. Temperatures and temperature ranges on DTA curves for phases obtained during hydration (ºC)

Reference	Year	CAH_{10}	C_2AH_8	C_3AH_6	AH_3	C_2ASH_8	AFm	Hc y Mc
[27]	1992	100-160	140-200	290-350	230**, 300**	190-230		
[28]	1983	~**140**	~**170**	**~300**	~**280**			
[29]	2000	110-160	**170, 270**	**289,450**	**181,3**			**86,**155,220
[30]	2007		88,**110**,**175**,**295**					
[31]	1988		145-150,265-280	**300**				160
[32]	1978	**~125**		**~330**	**~290**			
[33]	2013	**165**	**285**	285-451	~260-290			
[34]	2009	~100-170	~110-290	330	~300-470	120-185		
[35]	2003		240-285	290-300	260-270		180-200	
[36]	1976					120,**165**, **220**,**430**		
[37]	2016						190-200,270-290	
[38]	2012			**273**,400			120-170	**150**
This work	2017		**92**,150,**311**	**303**,425	239,**300**,**515**		120,180,295	

.

Table 8. Amount of hydrates determined by XRD and under hypothesis of all sulphate in solution giving AFm and all aluminium in excess forming strätlingite. Their corresponding lost of water. TG lost of mass

wt(%)	AFm	C_2ASH_8	AH_3	Lost of mass (water)	P (1000ºC)
	DRX/hip	DRX/hip	DRX/hip	DRX/hip	TG
$C_{12}A_7$+ $C_5S_2\bar{S}$	11.6 / 34	24.8 / 17.1	---	11.5 / 17.7	22
CA+ $C_5S_2\bar{S}$	5.8 / 30.4	36 / 40.9	---	12.8 / 21.1	25.3
$C_4A_3\bar{S}$+$C_5S_2\bar{S}$	10.6 / 29.3	---	- / 14	4.1 / 15.3	17.6

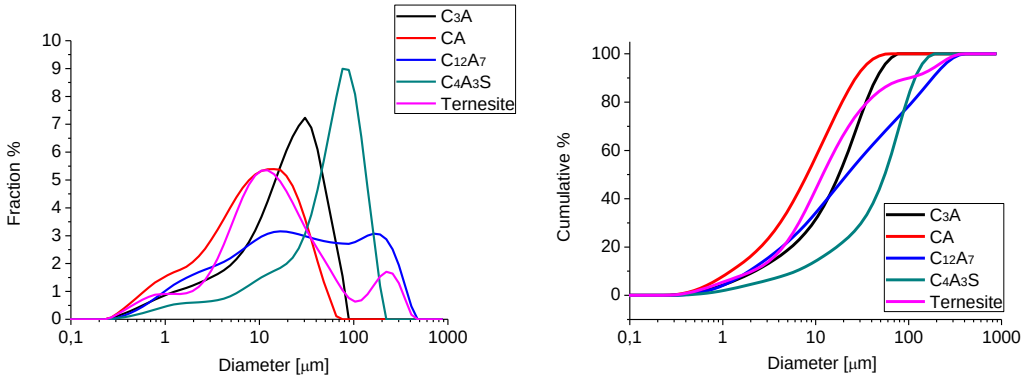

Figure 1. Particle size distribution (PSD) and the derivative of the PSD of samples C_3A, CA, $C_{12}A_7$, $C_4A_3\bar{S}$, and ternesite.

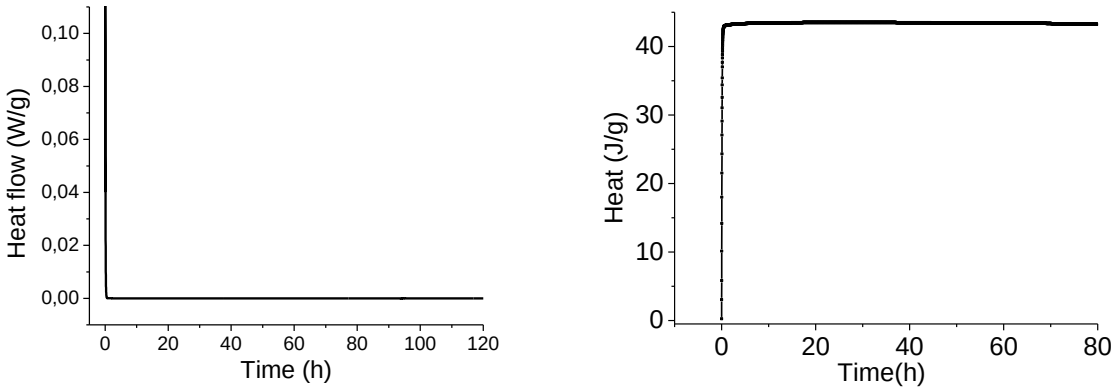

Figure 2. Heat flow and heat curves for 7 day (25ºC) ternesite hydration

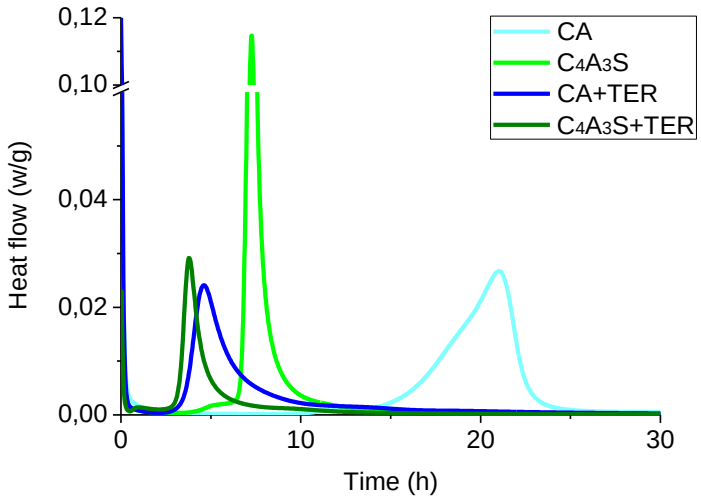

695)

696

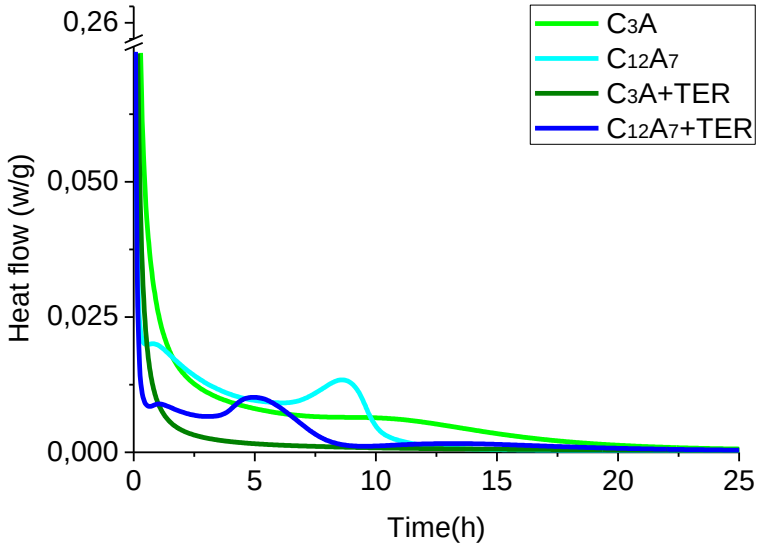

697 b)

698 Figure 3. Heat flow curves for synthesised aluminates and their ternesite blends pastes
699 at 25 °C

700

701

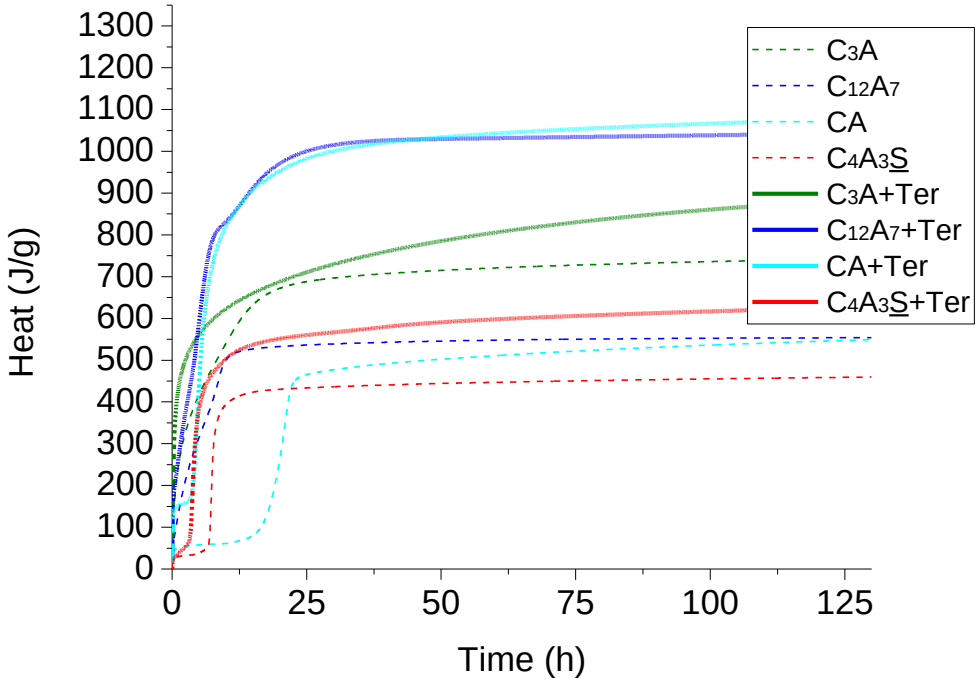

Figure 4. Heat of hydration curves for 7 d (25 °C) hydrated aluminates and their ternesite blends (per unit of mass of aluminate)

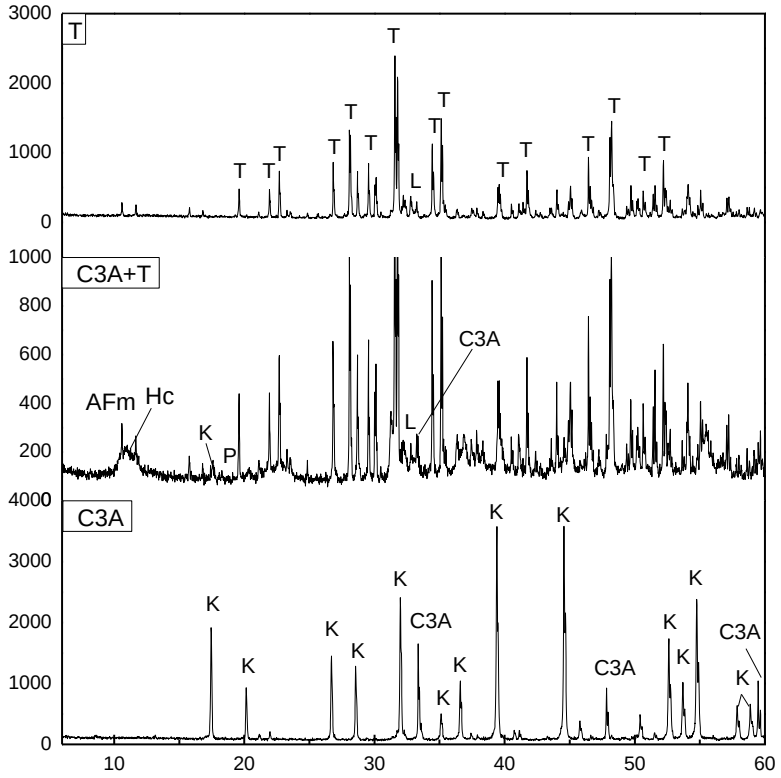

Figure 5. Diffractograms for 7 d (25 °C) C_3A and C_3A/ $C_5S_2\bar{S}$ (1:2) pastes: K = katoite; AFm= Calcium sulfoaluminate.L= larnite; T= ternesite; Hc = calcium hemicarboaluminate; P= portlandite

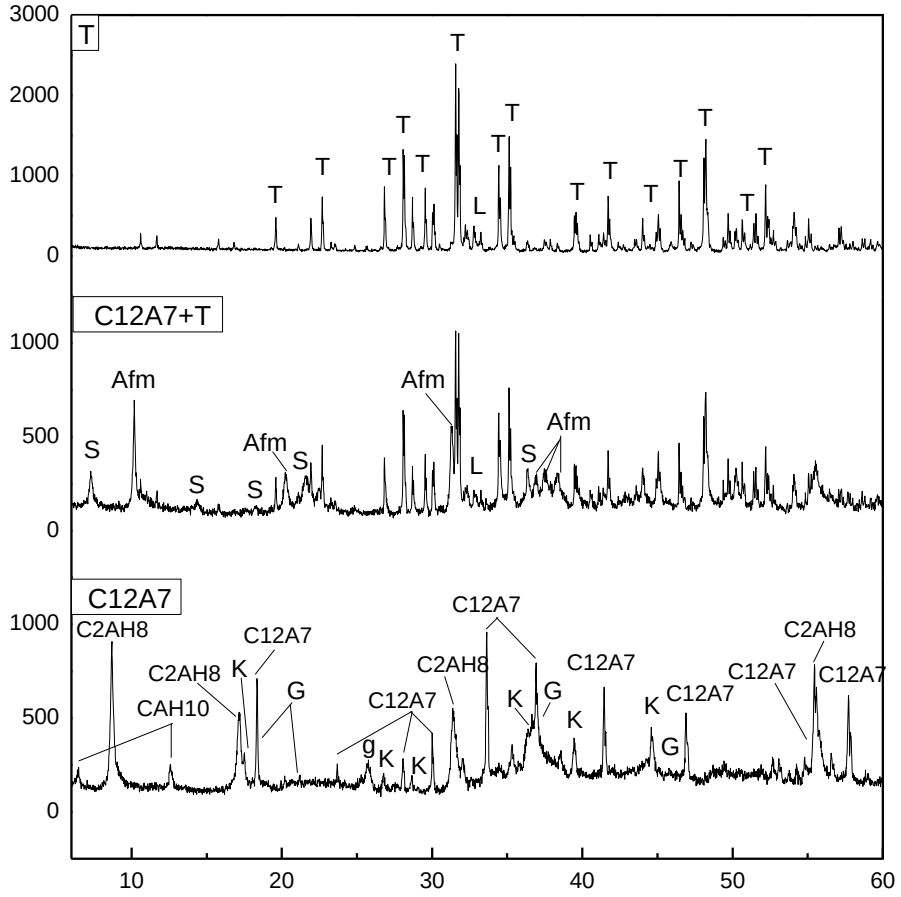

717
718 Figure 6. Diffractograms for 7 d (25 °C) $C_{12}A_7$ and $C_{12}A_7$/ $C_5S_2\bar{S}$ (1:2) pastes: K =
719 katoite; G= gibbsite; L= larnite; S= strätlingite; T= ternesite; Afm = calcium
720 monosulfoaluminate hydrate; g= grossite
721
722
723

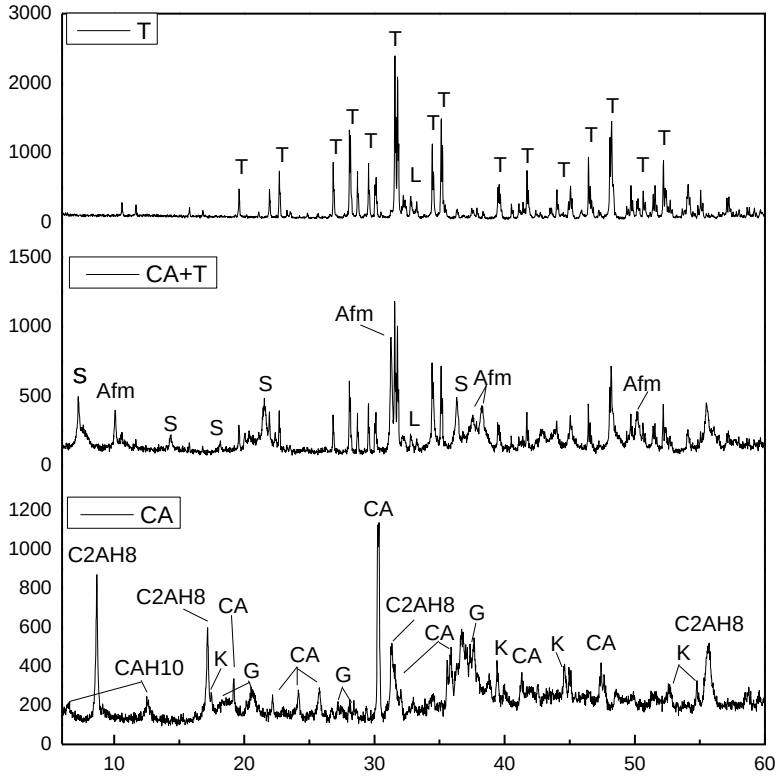

Figure 7. Diffractograms for 7 d (25 °C) CA and CA/$C_5S_2\hat{s}$ (1:2) pastes: K = katoite; G= gibbsite; L= larnite; T= ternesite; Afm = calcium monosulfoaluminate hydrate; S= strätlingite

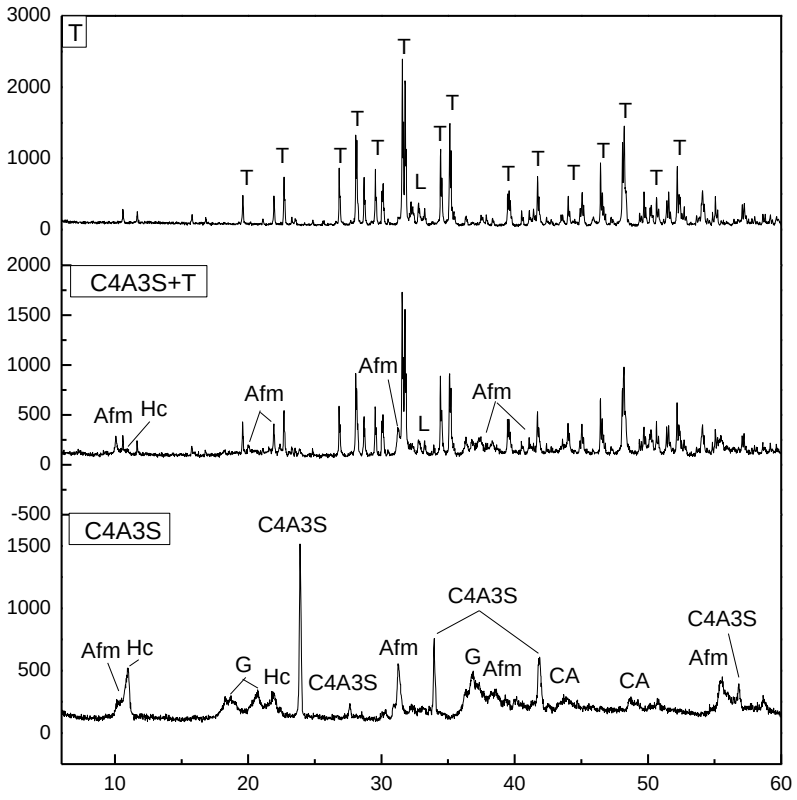

730
731 Figure 8. Diffractograms for 7 d (25 °C) $C_4A_3\bar{S}$ and $C_4A_3\bar{S}$/ $C_5S_2\bar{S}$ (1:2) pastes: =
732 gibbsite; L= larnite; T= ternesite; Afm = calcium monosulfoaluminate hydrate; Hc=
733 calcium monocarboaluminate hydrate
734
735

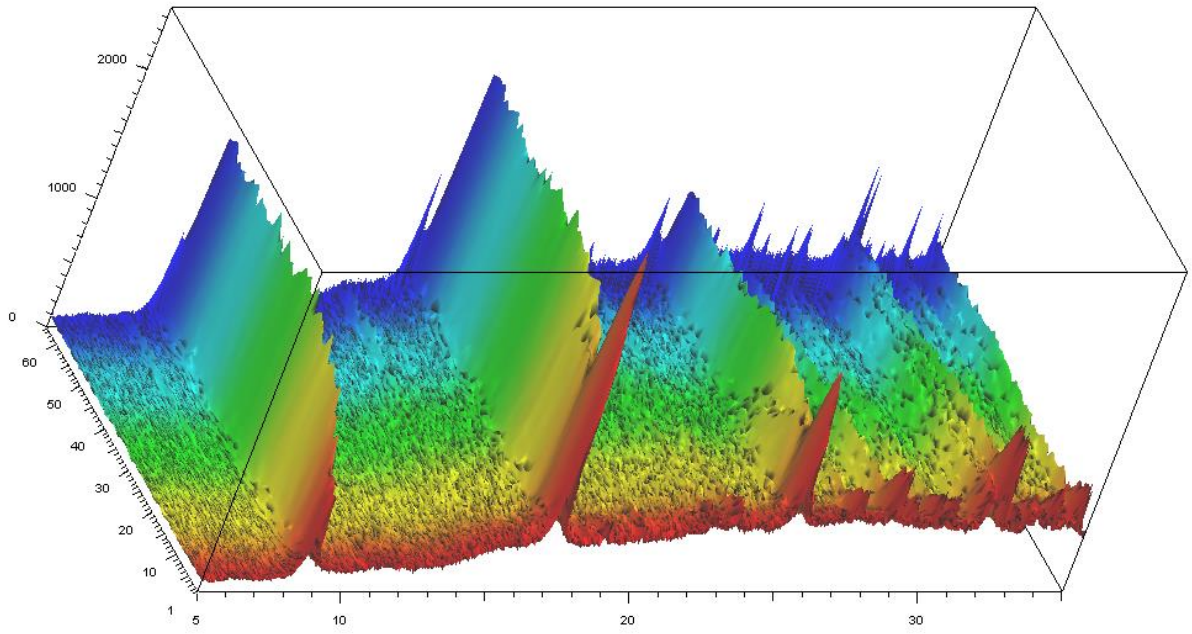

a) 1–64

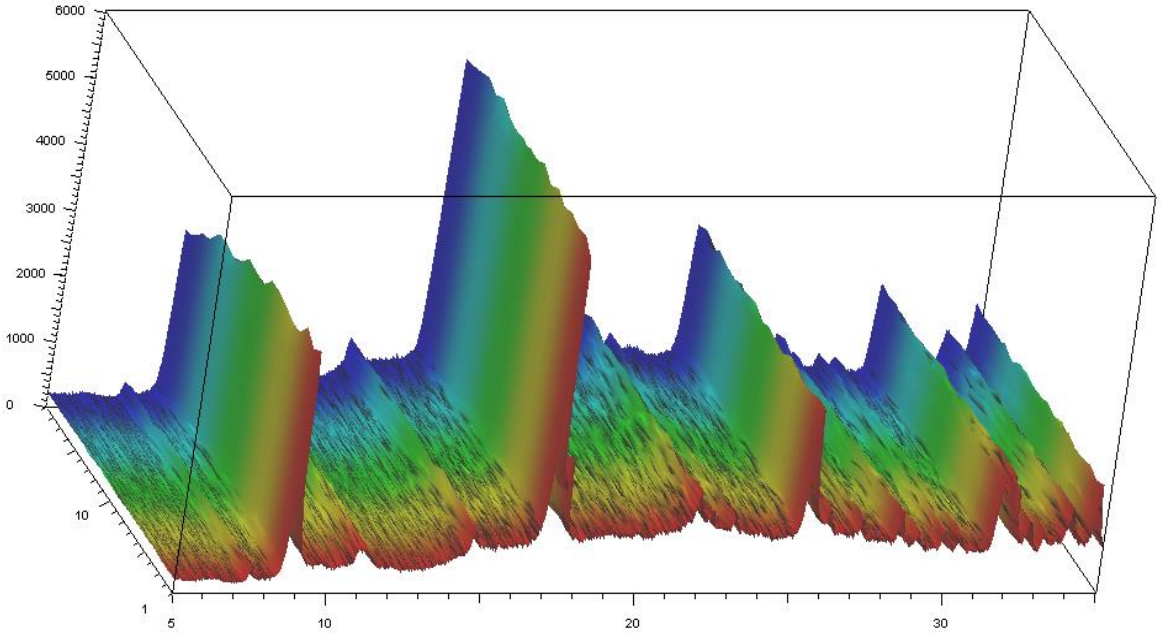

b) 65-84

Figure 9. Three-dimensional diffractograms for 0 h-20 h $C_{12}A_7$+ternesite pastes: a) samples 1-64 (0-12 h); b) samples 65-84 (12-20 h)

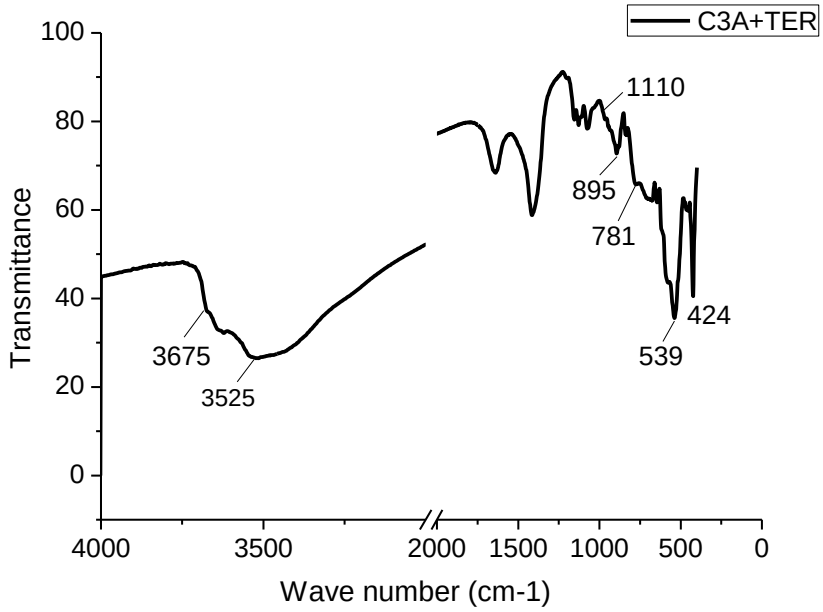

Figure 10. FTIR spectra for 7 d (25°C) C_3A+ternesite paste after subtracting the ternesite spectrum

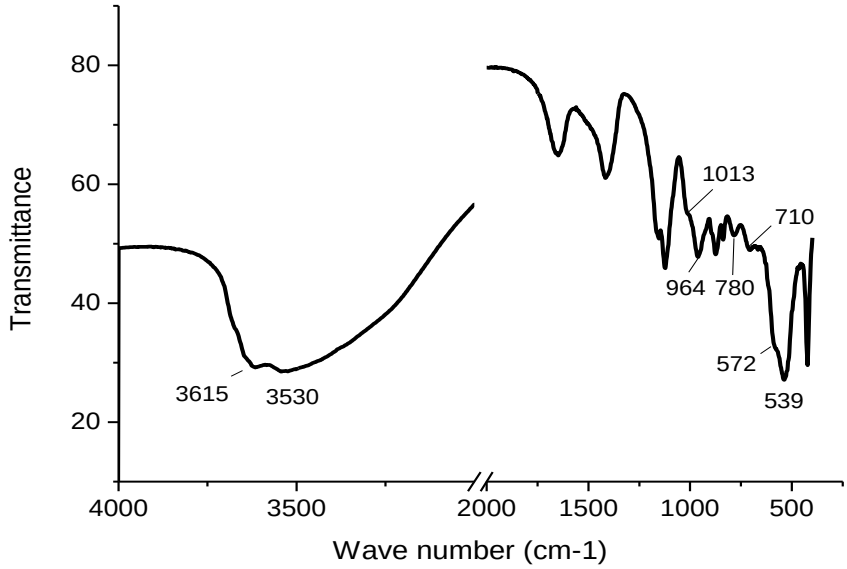

Figure 11. FTIR spectra for 7 d (25°C) $C_{12}A_7$+ternesite paste after subtracting the ternesite spectrum

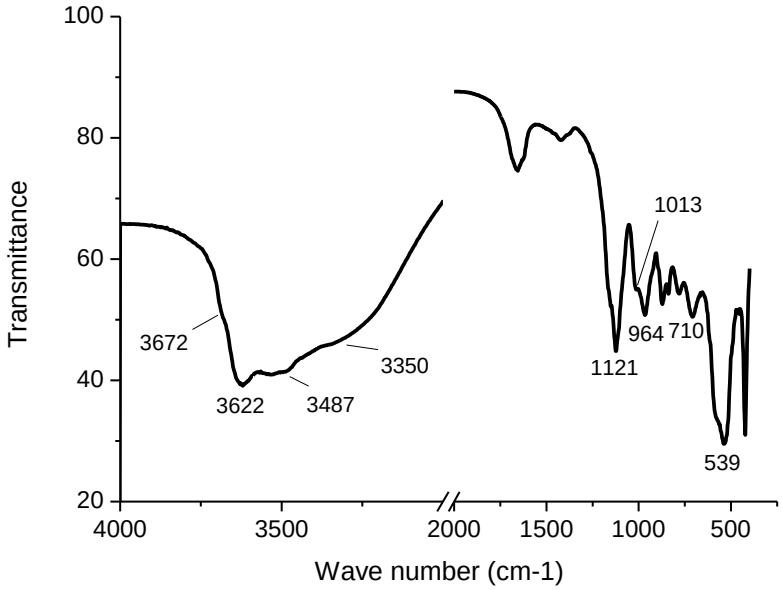

Figure 12. FTIR spectra for 7 d (25°C) CA+ternesite paste after subtracting the ternesite spectrum

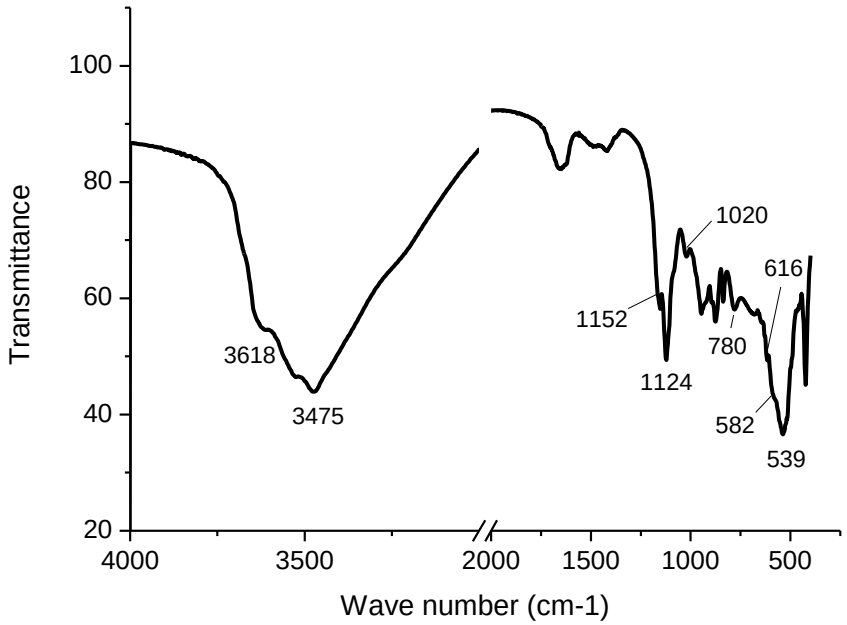

Figure 13. FTIR spectra for 7 d (25°C) $C_4A_3\bar{S}$+ternesite paste after subtracting the ternesite spectrum

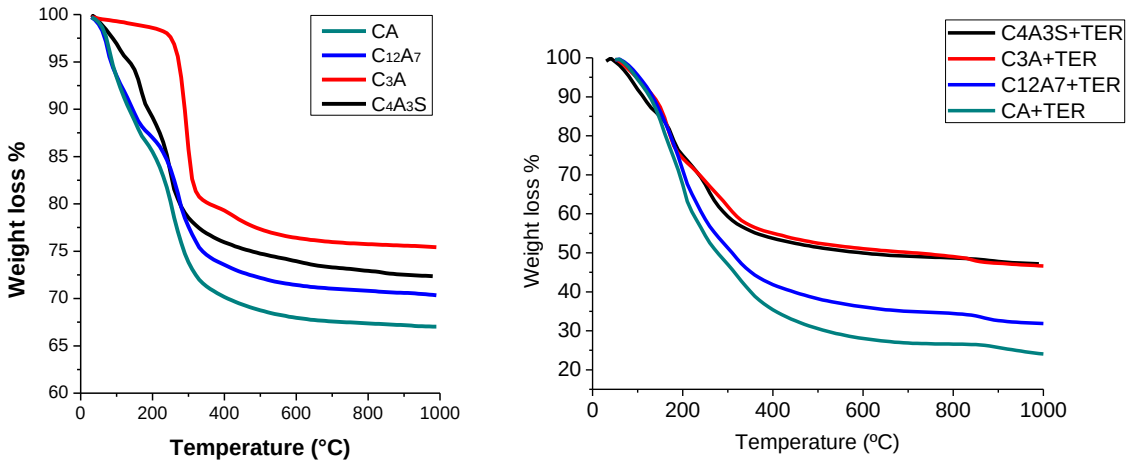

a) b)

Figure 14. a) Weight loss in aluminate pastes; b) weight loss in aluminate+ternesite pastes (per g of aluminate)

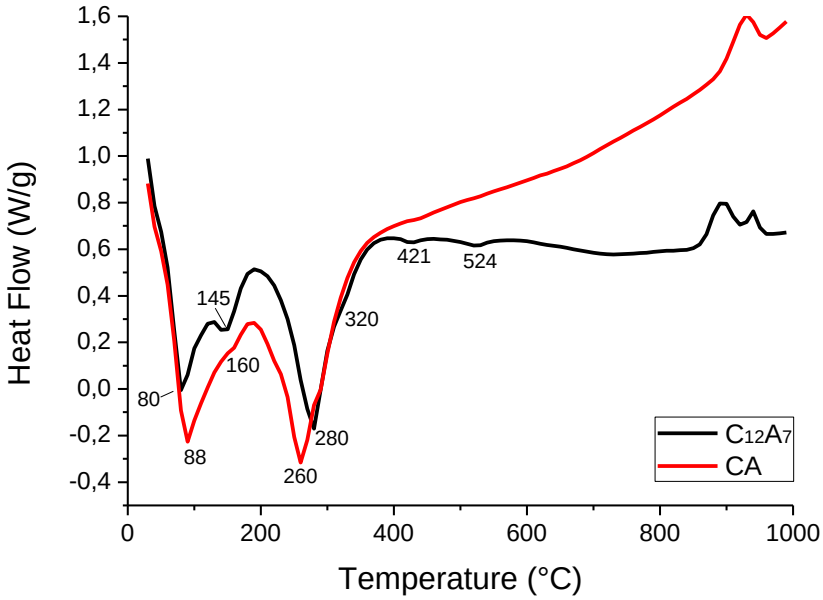

Figure 15. DTA curves for pastes CA and $C_{12}A_7$

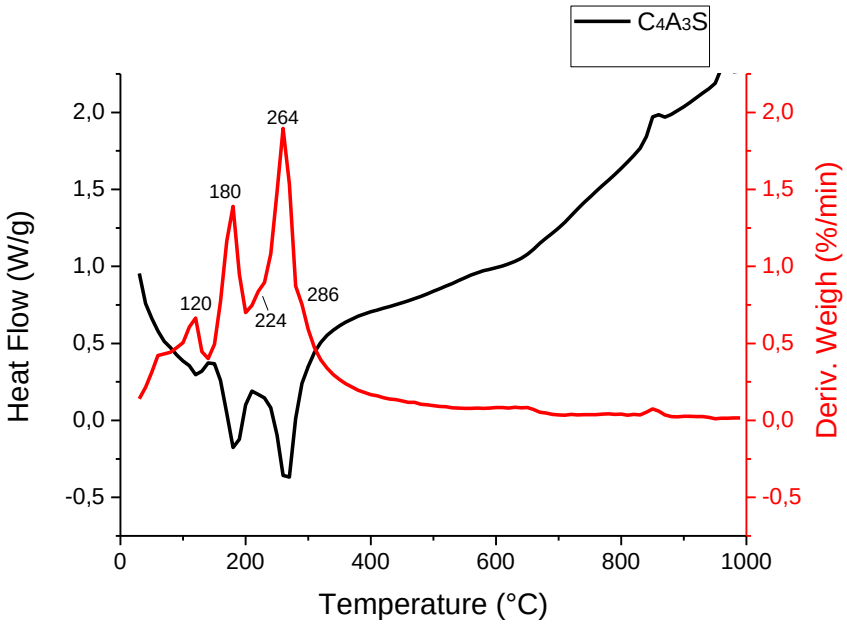

774
775 Figure 16.DTA curves for hydrated paste $C_4A_3\hat{s}$
776
777

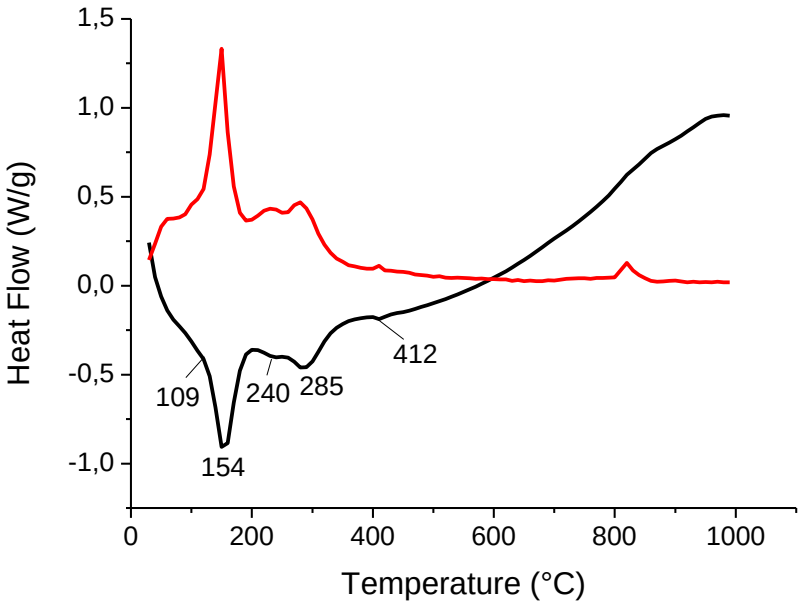

778
779 Figure 17.DTA curves for paste C_3A+ternesite
780

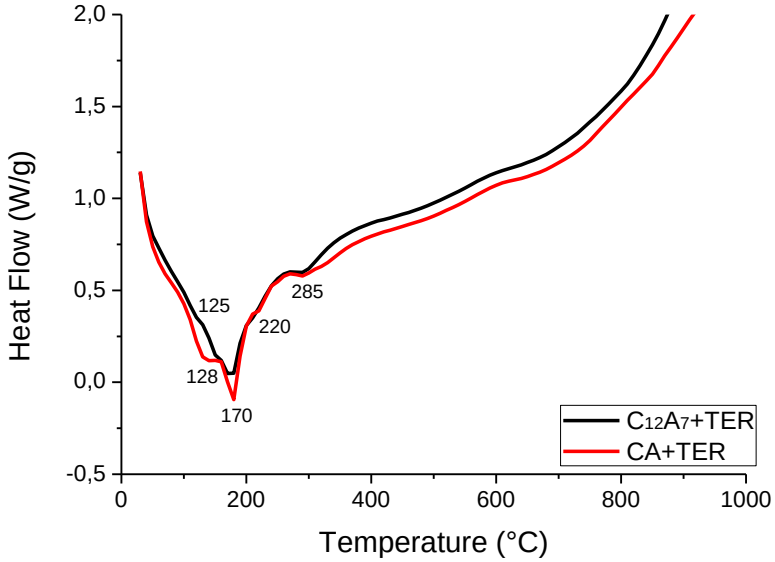

781
782 Figure 18.DTA curves for pastes CA+ternesite and $C_{12}A_7$+ternesite
783

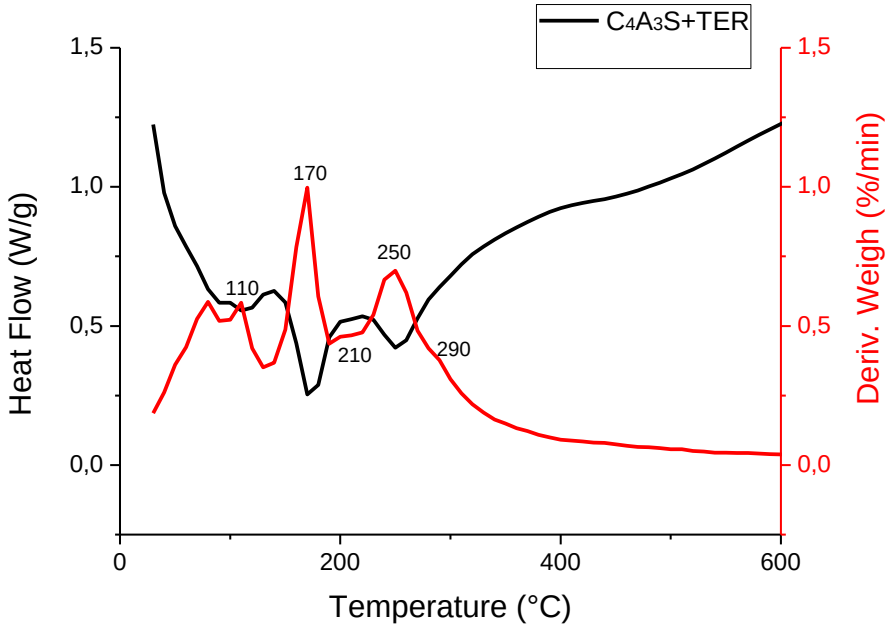

784
785 Figure 19.DTA curves for paste $C_4A_3\bar{S}$+ternesite
786
787